

## FIRST-PRINCIPLES STUDY ON THE MECHANICAL PROPERTIES OF $Al_3NiP_4$ UNDER STRAIN

by

**Yu CHEN\***

College of Science, Inner Mongolia University of Technology, Hohhot, China

Original scientific paper  
<https://doi.org/10.2298/TSCI2503803C>

*In this study, the mechanical properties of  $Al_3NiP_4$  were calculated by applying uniaxial strain in the *a*-direction. It has been demonstrated that when the strain reaches 27%, the requisite mechanical stability condition is not met. Consequently, the mechanical properties of  $Al_3NiP_4$  were examined exclusively within the strain range of 0% to 26%. The stress-strain curve of  $Al_3NiP_4$  under uniaxial strain revealed that the application of strain in the *a*-direction resulted in significantly greater stress in the *a*-direction than in the *b*- and *c*-directions. When the strain in the *a*-direction is less than 18%, the stress-strain curve exhibits a linear pattern that is representative of the expected behavior. When the strain exceeds 18%, a slight non-linear phenomenon is observed. Among all deformations,  $Al_3NiP_4$  exhibits elastic deformation without significant plastic deformation. Additionally, it was observed that stretching can modify the elastic modulus of  $Al_3NiP_4$ , enhance its Vickers hardness, and diminish its ductility. Our findings indicate that the mechanical properties of  $Al_3NiP_4$  can be regulated by applying uniaxial strain, thereby expanding the scope of applications for  $Al_3NiP_4$  materials.*

Key words: *first-principles, mechanical stability, strain, elastic modulus, Vickers hardness*

### Introduction

In the field of material science, alloys are commonly utilized in composite materials to enhance mechanical properties [1], and the first principles can be employed to optimize the composite [2]. The application of first principles has now been extended to inorganic materials in addition to metallic materials [3, 4]. By employing the first principles, Surthi *et al.* [5] devised nanofiber membranes through electrospinning, a technique utilized for the fabrication of diverse functional nanofibers [6, 7]. Furthermore, Mehta and Helmicki [8] proposed a first principles-based modeling approach for microdevices, which has the potential for extensive applications in sensors [9, 10].

Aluminum phosphide (AIP) is a significant III-V compound semiconductor material that has been extensively utilized in the development of functional materials [11, 12]. The doping of transition metals into AIP represents an effective method for the improvement of its mechanical, magnetic, and optical properties. A substantial body of research has been conducted on the magnetic and optical properties of the semiconductor  $Al_{1-x}TM_xP$  (where TM represents a transition metal, rare earth, or non-metal). However, there is a paucity of studies

\* Author's e-mail: [chenyu@imut.edu.cn](mailto:chenyu@imut.edu.cn)

on its mechanical properties [13-16]. The application of strain (hydrostatic pressure) to the material represents an effective method for the regulation of its magnetic properties and optical properties [17-23]. However, AlP is a brittle material, which makes it challenging to apply a significant response to it. In previous research, the author discovered that  $\text{Al}_3\text{NiP}_4$  exhibits excellent ductility. Accordingly, the present study will further examine its mechanical properties. The objective of this study is to apply uniaxial strain to  $\text{Al}_3\text{NiP}_4$ , examine its ultimate strain capacity, and investigate the regulatory effect of strain on its mechanical properties.

### Computational methods

In this study, we used the super helpful density functional theory to calculate the properties of  $\text{Al}_3\text{NiP}_4$  under uniaxial strain. We used a plane-wave pseudopotential method as implemented in the Cambridge Sequential Total Energy Package (CASTEP) code [24-26] to do this. We used the generalized gradient approximation (GGA) within the Perdew, Burke, and Ernzerhof scheme to obtain the exchange-correlation potential. To make sure our calculations were as precise as possible, we set the plane-wave energy cutoff to 400 eV and used Brillouin-zone of  $2 \times 2 \times 5$  Monkhorst-Pack mesh of  $k$  points. We also set the remaining parameters to their default ultra-fine accuracy settings.

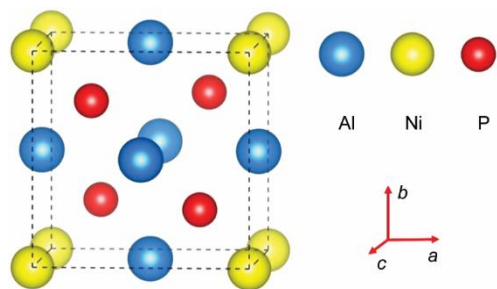


Figure 1. The supercell models of  $\text{Al}_3\text{NiP}_4$

In this study, the  $\text{Al}_3\text{NiP}_4$  ( $\text{Al}_{0.75}\text{Ni}_{0.25}\text{P}$ ) compound was obtained by substituting one Al atom with one Ni atom in a  $1 \times 1 \times 1$   $\text{Al}_4\text{P}_4$  supercell model, as illustrated in fig. 1. The lattice constants of  $\text{Al}_3\text{NiP}_4$  are  $a = 0.5298$  nm,  $b = 0.5298$  nm, and  $c = 0.5559$  nm.

For  $\text{Al}_3\text{NiP}_4$ , the mechanical properties are calculated under strain conditions by applying uniaxial strain in the  $a$ -direction. The calculation process is divided into three steps:

- *Set the corresponding uniaxial strain.* Set the lattice constant in CASTEP, and the ideal single axis strain is applied here, that is, there is only response in the direction of  $a$ , no response in the  $b$ - and  $c$ -directions, and the crystal constant of the  $b$ - and  $c$ -direction remains constant.
- *Geometric optimization of supercells.* Only optimizing atomic positions without optimizing lattice constants; This geometric optimization method enables the atoms in the lattice to get the most stable position and maintain the corresponding strain.
- Calculate mechanical stability, elastic properties, including elastic stiffness constant and elastic modulus.

### Results and discussion

#### Elastic constants and mechanical stability

The elastic constants of crystals serve to establish a correlation between mechanical and dynamical behaviors. Additionally, they provide crucial insight into the elastic response of a crystal to external pressure. The elastic constants are significant parameters for characterizing the mechanical properties of solids. The elastic matrix has dimensions  $6 \times 6$  and is symmetric. As the degree of crystal symmetry increases, the number of independent elastic stiffness constants decreases. A maximum of 21 independent elastic stiffness constants can be

identified. The elastic constants  $C_{ij}$ 's for the orthorhombic  $\text{Al}_3\text{NiP}_4$  supercell, as predicted by the GGA method. The elastic constants indicate that  $\text{Al}_3\text{NiP}_4$  is an orthorhombic crystal. The mechanical stability of a crystal structure under isotropic pressure can be determined by employing the criteria of independent elastic constants,  $C_{ij}$ . In the case of an orthorhombic crystal, the independent components are as follows, as demonstrated in the following equation [27, 28]:

$$\begin{aligned} C_{ii} &> 0 \\ C_{11} + C_{22} - 2C_{12} &> 0 \\ C_{11} + C_{33} - 2C_{13} &> 0 \\ C_{22} + C_{33} - 2C_{23} &> 0 \\ C_{11} + C_{22} + C_{33} + 2(C_{12} + C_{13} + C_{23}) &> 0 \end{aligned} \quad (1)$$

A review of the literature reveals that when the strain reaches 27%, the mechanical stability condition is not met. Accordingly, an investigation into the mechanical properties of  $\text{Al}_3\text{NiP}_4$  was only conducted when the strain was within the range of 0% to 26%.

#### Stress-strain curve

The stress-strain curve depicts the variation in stress with strain during solid deformation. In accordance with Hooke's law, the formula for calculating the stress-strain curve for uniaxial strain can be derived. In this context, the symbol  $\sigma_a$  ( $\sigma_b$ ,  $\sigma_c$ ) represents stress, while  $\Delta a$  represents strain increment in the  $a$ -direction.

$$\begin{aligned} (\sigma_a)_i &= (\sigma_a)_{i-1} + C_{11}\Delta a \\ (\sigma_b)_i &= (\sigma_b)_{i-1} + C_{12}\Delta a \\ (\sigma_c)_i &= (\sigma_c)_{i-1} + C_{13}\Delta a \end{aligned} \quad (2)$$

As illustrated in fig. 2, the stress-strain curve of  $\text{Al}_3\text{NiP}_4$  under uniaxial strain can be obtained using eq. (2). The application of strain in the  $a$ -direction results in a markedly elevated stress in the  $a$ -direction relative to the  $b$ -direction and  $c$ -direction. When the strain in direction  $a$  is less than 18%, the stress-strain curve exhibits a linear pattern that is representative of the expected behavior. Upon exceeding a strain of 18%, a slight non-linear phenomenon becomes evident. From the outset, the  $b$ -directions and  $c$ -directions display non-linear effects. Prior to reaching a strain of 6%, the stress in the  $b$ -direction is observed to exceed that in the  $c$ -direction. Upon reaching a strain of 6%, the stress in the  $c$ -direction is observed to exceed that in the  $b$ -direction. At all stages of deformation,  $\text{Al}_3\text{NiP}_4$  displays elastic behaviour, with no discernible plastic deformation.

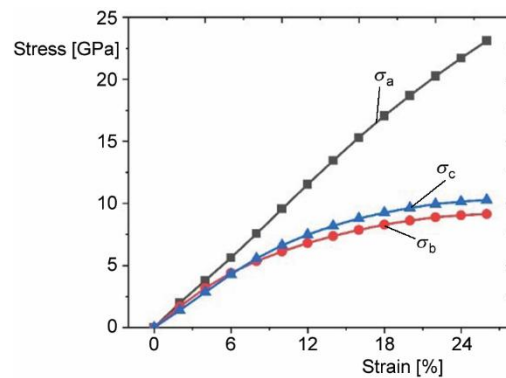


Figure 2. The stress-strain curve of  $\text{Al}_3\text{NiP}_4$  in  $a$ -direction uniaxial strain

*Elastic modulus*

The elastic modulus of polycrystalline materials is inextricably linked to the elastic constants of single crystals. In general, the elastic properties of polycrystalline materials are of greater practical significance than those of single crystals, which makes them incredibly useful in a wide range of applications. The elastic properties of polycrystalline materials are defined by four key values: the bulk modulus  $B$ , the shear modulus  $G$ , the Young's modulus  $E$ , and the Poisson ratio,  $\mu$ . Fortunately, there are two excellent models available for evaluating the modulus: the Voigt method and the Reuss method. The former provides an upper bound, while the latter provides a lower bound for the polycrystalline elastic modulus. The fantastic news is that the bulk modulus and shear modulus according to Voigt can be expressed for different crystalline systems as follows [29, 30]:

$$B_V = \frac{C_{11} + C_{22} + C_{33} + 2(C_{12} + C_{13} + C_{23})}{9} \quad (3)$$

$$G_V = \frac{C_{11} + C_{22} + C_{33} - C_{12} - C_{13} - C_{23}}{15} + \frac{C_{44} + C_{55} + C_{66}}{5} \quad (4)$$

and by Reuss that:

$$B_R = \frac{1}{S_{11} + S_{22} + S_{33} + 2(S_{12} + S_{13} + S_{23})} \quad (5)$$

$$G_R = \frac{15}{4(S_{11} + S_{22} + S_{33}) + 3(S_{44} + S_{55} + S_{66}) - 4(S_{12} + S_{13} + S_{23})} \quad (6)$$

Voigt-Reuss-Hill method can be used to get the bulk modulus and shear modulus. The widely used estimate for the theoretical value of the polycrystalline elastic modulus is the Voigt-Reuss-Hill average, which is found by taking the arithmetic mean of the Voigt and Reuss bounds:

$$B = \frac{B_V + B_R}{2} \quad (7)$$

$$G = \frac{G_V + G_R}{2} \quad (8)$$

The Young's modulus and Poisson's ratio can be calculated based on the aforementioned values using the following formulas:

$$E = \frac{9BG}{3B + G} \quad (9)$$

$$\mu = \frac{3B - 2G}{6B + 2G} \quad (10)$$

The  $B$ ,  $G$ ,  $E$  and  $\mu$  of  $\text{Al}_3\text{NiP}_4$  are calculated in accordance with the prescribed eqs. (3)-(10). The resulting calculations are presented in fig. 3.

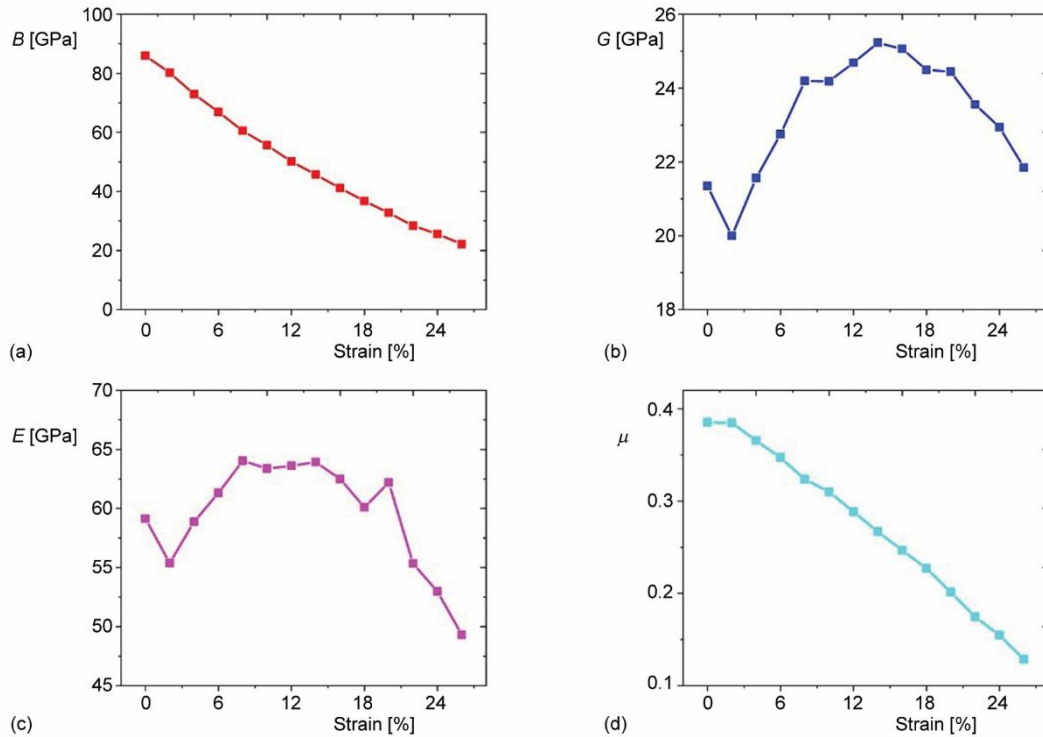


**Figure 3.** (a) The bulk modulus of  $\text{Al}_3\text{NiP}_4$ , (b) the shear modulus of  $\text{Al}_3\text{NiP}_4$ , (c) the Young's modulus of  $\text{Al}_3\text{NiP}_4$ , and (d) the Poisson's ratio of  $\text{Al}_3\text{NiP}_4$

Figure 3(a) illustrates the change of the bulk modulus  $B$  of  $\text{Al}_3\text{NiP}_4$  with strain. The overall trend is a decrease, with a minimum value of approximately 26% in the absence of strain.

The change of the shear modulus  $G$  of  $\text{Al}_3\text{NiP}_4$  with strain is illustrated in fig. 3(b). The data exhibit an approximately arched trend, with a maximum value at a strain of 14%, which is approximately 1.2 times that at no strain.

The change of the Young's modulus  $E$  of  $\text{Al}_3\text{NiP}_4$  with strain is illustrated in fig. 3(c). It demonstrates an approximately arched trend, with a maximum value at a strain of 8%, which is approximately 1.1 times that at no strain.

The change of the Poisson ratio  $\mu$  of  $\text{Al}_3\text{NiP}_4$  with strain is illustrated in fig. 3(d). The overall trend is a decrease, with a minimum value of approximately 33% in the absence of strain.

#### *Vickers hardness and ductility*

Vickers hardness is a useful concept that defines a material intrinsic resistance to deformation when a force is applied. The formal theoretical definition of hardness is still a challenge for those engaged in the scientific study of materials. The hardness of a material is related to its elastic and plastic properties, which makes it an intriguing topic of study. Several semi-empirical models have been developed to predict the hardness of materials, and one of the most promising is the model put forth by Chen *et al.* [31] for forecasting the hardness of polycrystalline materials and bulk metallic glasses. This model is based on the Pugh modulus

ratio ( $k = G/B$ ) and the shear modulus, as detailed in reference [31], and it has the potential to revolutionize our understanding of material hardness:

$$H_V = 1.887k^{1.171}G^{0.591} \quad (11)$$

where  $H_V$  denotes the Vickers hardness.

The  $B/G$  ratio can be employed to gauge the ductility or brittleness of materials, as a high (low) value is correlated with ductility (brittleness). The critical value is approximately 1.75 [32]:

$$D = \frac{B}{G} \quad (12)$$

The  $H_V$  and  $B/G$  of  $Al_3NiP_4$  are calculated in accordance with eqs. (11) and (12). The resulting calculations are presented in fig. 4.

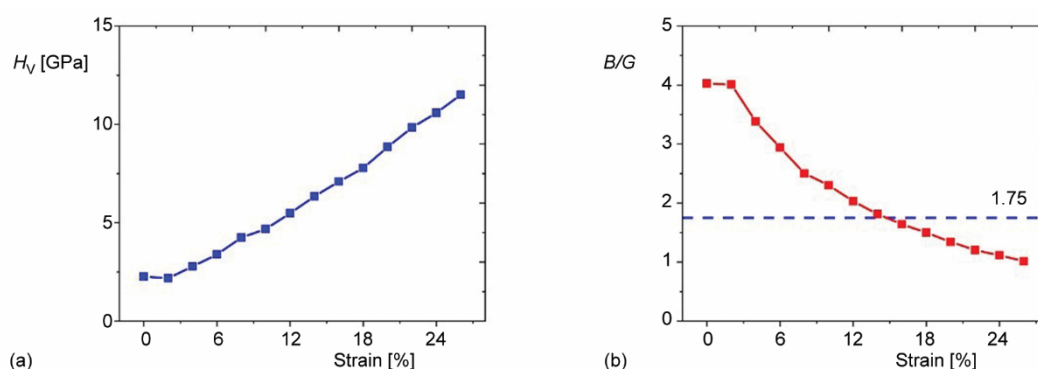


Figure 4. (a) The  $H_V$  of  $Al_3NiP_4$  and (b) the  $B/G$  of  $Al_3NiP_4$

The variation law of the Vickers hardness of  $Al_3NiP_4$  with strain is shown in fig. 4(a). The overall trend is upward, with a maximum value at a strain of 26%, which is approximately 5.1 times that at no strain.

The variation law of the  $B/G$  of  $Al_3NiP_4$  with strain is shown in fig. 4(b). The overall trend is decreasing, with a minimum value of about 25% when there is no strain. When the strain is less than 14%,  $Al_3NiP_4$  expressing better ductility, when the strain is greater than 16%,  $Al_3NiP_4$  expressing better brittleness.

## Conclusion

In this study, the mechanical properties of  $Al_3NiP_4$  were calculated by applying uni-axial strain in the  $a$ -direction. The findings indicate that  $Al_3NiP_4$  exhibits a limit strain of 26% and a linear strain range of 18%, rendering it an optimal material for the fabrication of large deformation strain sensors [33]. Moreover, the elastic modulus, Vickers hardness, and ductility of  $Al_3NiP_4$  can be modified by the applied strain. The adjustable properties of elasticity permit the extension of the material application range. The findings of this study suggest that  $Al_3NiP_4$  is a material with potential engineering applications.

## Acknowledgment

The research work is supported by the Research Program of Science and Technology at Universities of Inner Mongolia Autonomous Region (NJZY22389) and the Scientific Research Project of Inner Mongolia University of Technology (BS2021058).

## References

- [1] Liovic, D., *et al.*, Surface Roughness of Ti<sub>6</sub>Al<sub>4</sub>V Alloy Produced by Laser Powder Bed Fusion, *Facta Universitatis Series: Mechanical Engineering*, 22 (2024), 1, pp. 63-76
- [2] Jiang, A. F., Chen, Y., First-Principles Study on the Mechanical Properties of Al<sub>1-x</sub>TM<sub>x</sub>P, *Thermal Science*, 28 (2024), 3A, pp. 2277-2285
- [3] Liu, S., *et al.*, Intrinsic Ferroelectric Switching from First Principles, *Nature*, 534 (2016), June, pp. 360-363
- [4] Honkala, K., *et al.*, Ammonia Synthesis from First-Principles Calculations, *Science*, 307 (2005), Jan., pp. 555-558
- [5] Surthi, K. K., *et al.*, SU8 Polymer Derived High Capacity and Performance Anode Material for Secondary and Flexible Li-Ion Batteries: Experimental and First Principle Study, *Chemical Engineering Journal*, 479 (2024), 147561
- [6] Qian, M. Y., He, J.-H., Collection of Polymer Bubble As A Nanoscale Membrane, *Surfaces and Interface*, 28 (2022), 101665
- [7] Zuo, Y. T., Liu, H. J., Is the Spider a Weaving Master or a Printing Expert? *Thermal Science*, 26 (2022), 3B, pp. 2471-2475
- [8] Mehta, A., Helmicki, A. J., First Principles Based Approach to Modeling of Microfluidic Systems, *Proc. Microfluidic Devices and Systems*, 3515 (1998), 322087
- [9] He, J.-H., *et al.*, Piezoelectric Biosensor Based on Ultrasensitive MEMS System, *Sensors and Actuators A: Physical*, 376 (2024), 115664
- [10] He, J.-H., Periodic Solution of a Micro-Electromechanical System, *Facta Universitatis, Series: Mechanical Engineering*, 22 (2024), 2, pp. 187-198
- [11] Sajjad, M., *et al.*, First Principles Study of Structural, Elastic, Electronic and Magnetic Properties of Mn-doped AlY (Y = N, P, As) Compounds, *Journal of Magnetism and Magnetic Materials*, 390 (2015), Sept., pp. 78-86
- [12] Wang, S., *et al.*, Room-Temperature Ferromagnetism in Alkaline-Earth-Metal Doped AIP: First-Principle Calculations, *Computational Materials Science*, 142 (2018), Feb., pp. 338-345
- [13] Zhang, Y., *et al.*, Half-Metallic Ferromagnetism in Cr-doped AIP-density Functional Calculations, *Solid State Communications*, 145 (2008), Mar., pp. 590-593
- [14] Yang, R., *et al.*, First-Principles Study on Phases of AIP, *Solid State Communications*, 267 (2017), Nov., pp. 23-28
- [15] Yan, Z., *et al.*, Ferromagnetism in Alkali-Metal-Doped AIP: An ab Initio Study, *Computational Materials Science*, 99 (2015), Mar., pp. 16-20
- [16] Boutaleb, M., *et al.*, Half-Metallic Ferromagnetic Properties of Cr- and V-doped AIP Semiconductors, *Journal of Magnetism and Magnetic Materials*, 397 (2016), Jan., pp. 132-138
- [17] Akbari, A., *et al.*, Tuning the Electronic and Optical Properties of XP (X = Al, Ga) Monolayer Semiconductors Using Biaxial Strain Effect: Modified Becke-Johnson Calculations, *Chemical Physics Letters*, 691 (2018), Jan., pp. 181-189
- [18] Webster, L., Yan, J., Strain-Tunable Magnetic Anisotropy in Monolayer CrCl<sub>3</sub>, CrBr<sub>3</sub>, and CrI<sub>3</sub>, *Physical Review B*, 98 (2018), 144411
- [19] Yang, J., *et al.*, Tuning Magnetic Properties of Cr<sub>2</sub>M<sub>2</sub>C<sub>3</sub>T<sub>2</sub> (M = Ti and V) Using Extensile Strain, *Computational Materials Science*, 139 (2017), Nov., pp. 313-319
- [20] Jalilian, J., Naseri, M., Elastic, Electronic and Optical Properties of Cubic Mg<sub>2</sub>C Under Hydrostatic Pressure: Modified Becke-Johnson Calculations, *Optik*, 136 (2017), May, pp. 411-420
- [21] Karimi, M. J., *et al.*, Linear and Non-Linear Optical Properties of Multilayered Spherical Quantum Dots: Effects of Geometrical Size, Hydrogenic Impurity, Hydrostatic Pressure and Temperature, *Journal of Luminescence*, 145 (2014), Jan., pp. 55-60
- [22] Lin, Y., *et al.*, Effect of Fe Doping on Structural, Elastic and Electronic Properties of B<sub>2</sub>ZrCu Phase Under Hydrostatic Pressure: A First-Principles Study, *Materials Chemistry and Physics*, 272 (2021), 124978

- [23] Rezaei, G., *et al.*, Electromagnetically Induced Transparency in a Two-Dimensional Quantum dot: Effects of Impurity, External Fields, Hydrostatic Pressure and Temperature, *Physica E*, 62 (2014), Aug., pp. 104-110
- [24] Bao, L., *et al.*, Revealing the Elastic Properties and Anisotropies of Mg<sub>2</sub>X (X = Si, Ge and Sn) with Different Structures from a First-Principles Calculation, *Materials Today Communications*, 24 (2020), 101337
- [25] Kushwaha, A. K., *et al.*, First Principles Investigations of Structural, Elastic, Mechanical, Electronic and Optical Properties of Triple Perovskite Ba<sub>2</sub>K<sub>2</sub>Te<sub>2</sub>O<sub>9</sub>, *Physica B: Condensed Matter*, 596 (2020), 412404
- [26] Lakel, S., *et al.*, Optical and Electronic Properties of B<sub>x</sub>Al<sub>1-x</sub>P Alloys: A First Principles Study, *Optik* 127 (2016), 8, pp. 3755-3761
- [27] Wu, Z., *et al.*, Crystal Structures and Elastic Properties of Superhard IrN<sub>2</sub> and IrN<sub>3</sub> from First Principles, *Physical Review B*, 76 (2007), 054115
- [28] Mouhat, F., Coudert, F., Necessary and Sufficient Elastic Stability Conditions in Various Crystal Systems, *Physical Review B*, 90 (2014), 224104
- [29] Li, L., *et al.*, First-Principle Calculations of Structural, Elastic and Thermodynamic Properties of Fe-B Compounds, *Intermetallics*, 46 (2014), Mar., pp. 211-221
- [30] Li, L. H., *et al.*, First-Principle and Molecular Dynamics Calculations for Physical Properties of Ni-Sn Alloy System, *Computational Materials Science*, 99 (2015), Mar., pp. 274-284
- [31] Zhou, X., *et al.*, Mechanical Properties and Electronic Structure of anti-ReO<sub>3</sub> Structured Cubic Nitrides, M<sub>3</sub>N, of *d* Block Transition Metals M: An *ab Initio* Study, *Journal of Alloys and Compounds*, 595 (2014), May, pp. 80-86
- [32] Shao, P., *et al.*, Structural, Electronic and elastic Properties of the Shape Memory Alloy NbRu: First-Principle Investigations, *Journal of Alloys and Compounds*, 695 (2017), Feb., pp. 3024-3029
- [33] Ha, H., *et al.*, Sensing Mechanism and Application of Mechanical Strain Sensor: A Mini-Review, *Facta Universitatis-series Mechanical Engineering*, 21 (2023), 4, pp. 751-772